Available online at www.sciencedirect.com
ScienceDirect
Journal of Power Sources 180 (2008) 122–131
JOURNAL OF POWER SOURCES
www.elsevier.com/locate/jpowsour

Effect of CO and CO_2 impurities on performance of direct hydrogen polymer-electrolyte fuel cells

R.K. Ahluwalia*, X. Wang

Nuclear Engineering Division, Argonne National Laboratory, Argonne, IL 60439, United States

Received 17 December 2007; received in revised form 25 January 2008; accepted 25 January 2008
Available online 16 February 2008

Abstract

Mechanisms by which trace amounts of CO and CO_2 impurities in fuel may affect the performance of direct hydrogen polymer-electrolyte fuel cell stacks have been investigated. It is found that the available data on CO-related polarization losses for Pt electrodes could be explained on the basis of CO adsorption on bridge sites, if the CO concentration is less than about 100 ppm, together with electrochemical oxidation of adsorbed CO at high overpotentials. The literature data on voltage degradation due to CO_2 is consistent with CO production by the reverse water–gas shift reaction between the gas phase CO_2 and the H_2 adsorbed on active Pt sites. The effect of oxygen crossover and air bleed in "cleaning" of poisoned sites could be modeled by considering competitive oxidation of adsorbed CO and H by gas phase O_2. A model has been developed to determine the buildup of CO and CO_2 impurities due to anode gas recycle. It indicates that depending on H_2 utilization, oxygen crossover and current density, anode gas recycle can enrich the recirculating gas with CO impurity but recycle always leads to buildup of CO_2 in the anode channels. The buildup of CO and CO_2 impurities can be controlled by purging a fraction of the spent anode gas. There is an optimum purge fraction at which the degradation in the stack efficiency is the smallest. At a purge rate higher than the optimum, the stack efficiency is reduced due to excessive loss of H_2 in purge gas. At a purge rate lower than the optimum, the stack efficiency is reduced due to the decrease in cell voltage caused by the excessive buildup of CO and CO_2. It is shown that the poisoning model can be used to determine the limits of CO and CO_2 impurities in fuel H_2 for a specified maximum acceptable degradation in cell voltage and stack efficiency. The impurity limits are functions of operating conditions, such as pressure and temperature, and stack design parameters, such as catalyst loading and membrane thickness.

Keywords: Polymer-electrolyte fuel cells; Fuel impurities; Hydrogen quality

1. Introduction

Whereas Pt electrodes in low-temperature polymer-electrolyte fuel cells (PEFC) show very small polarization losses for the hydrogen oxidation reaction, the losses can be significant if the fuel H_2 is not pure but contains small amounts of CO [1]. Furthermore, because automotive PEFC stacks operate at substantially less than 100% H_2 utilization per pass, the spent anode gas containing unconverted H_2 must be recycled to the anode inlet and, thus, may enrich in CO and other impurities, if they are present. Natural factors that limit the buildup of CO in anode channels include electrochemical oxidation of CO to CO_2 at high overpotentials and its reaction with O_2 that crosses over from the cathode channels. Also, the buildup of CO and other impurities can be actively controlled by purging a fraction of the spent anode gas recirculated to the anode inlet, albeit at the expense of H_2 that is lost with the purge gas.

Hydrogen produced by reforming hydrocarbons may contain CO_2 in addition to CO and other reactive and inert impurities. Carbon dioxide is not adsorbed as strongly on Pt as CO but is not completely inert either. The mechanism of CO_2 poisoning of the Pt catalyst may involve CO_2 reduction to CO by H_2 either electrochemically or through the reverse water–gas shift reaction.

The purpose of this paper is to analyze the effects of trace CO and CO_2 impurities in fuel H_2 on the performance of the PEFC stacks for automotive applications. More specifically, the purpose is to address the following questions related to these impurities:

* Corresponding author. Tel.: +1 630 252 5979; fax: +1 630 252 5287.
E-mail address: walia@anl.gov (R.K. Ahluwalia).

0378-7753/$ – see front matter © 2008 Elsevier B.V. All rights reserved.
doi:10.1016/j.jpowsour.2008.01.087

Nomenclature

A	membrane area
E	potential (or activation energy)
f_p	purge fraction
F	Faraday constant
ΔH	enthalpy of desorption
J	current density
k	rate constant
M	active sites
$\dot{N}$	molar flow rate
N_c	catalyst site density
P	pressure
R	gas constant (or recycle ratio)
T	temperature
V	cell voltage
z	charge transfer

Greek letters

α	anodic transfer coefficient
α_m	coefficient of net water transport across membrane
β	symmetry factor
δ	thickness
η	overpotential
λ	water content of membrane
θ	fractional coverage
ψ	permeance

Subscripts/superscripts

a	anode (or adsorption)
ae	anode electrode
c	cathode
ce	cathode electrode
d	desorption
e	electronic (or electrochemical)
g	gas
i	ionic
m	membrane
N	Nernst
p	bipolar plate
r	reaction (or reverse reaction)
ref	reference
s	activation (or surface reaction)

(a) What are the mechanisms by which CO and CO_2 impurities in fuel H_2 affect the performance of fuel cells?
(b) What is the effect of anode gas recycle on buildup of these impurities?
(c) How does the buildup of CO and CO_2 depend on purge rate?
(d) What is the effect of the buildup of impurities on cell voltage?
(e) What are the impacts of purge and impurity buildup on stack efficiency?
(f) What might be the "acceptable" levels of these impurities in fuel H_2?

The focus of this work is on the types of Pt electrodes and structures that are being considered for automotive direct-H_2 fuel cells. As such, we have not considered alloys in which a second element, such as Ru, Sn, or Mo, is added to improve the CO tolerance of the Pt catalyst. These types of alloys are more suitable for fuel cells operating with reformate streams that may contain impurities at higher concentrations than in fuel-cell quality hydrogen. In validating our model, we have used published experimental data obtained with finely dispersed Pt on high-surface area carbon supports. With some modifications, our model may be applicable to other electrode structures, such as nanostructured thin film catalysts, and alloys in which the second (or third) element is added to improve the mass activity and durability of Pt.

2. Model formulation

As briefly outlined in Refs. [2,3], we solve a set of equations for

(a) the ionic and electronic potential distributions,
(b) current generation in the catalyst layers,
(c) ionic and electronic current distributions,
(d) water transport across the polymer-electrolyte membrane,
(e) H_2, O_2, N_2 and H_2O concentrations across the porous catalyst and gas diffusion media layers,
(f) species concentrations in the gas channels, and
(g) capillary transport of liquid water across the porous media.

From these solutions, we determine the Nernst potential, E_N, and the overpotentials, η, in terms of which the cell voltage V can be written as

$$V = E_N - \eta_e^{ae} - \eta_g^{ae} - \eta_e^a - \eta_i^a - \eta_g^a - \eta_s^a - \eta_i^m - \eta_e^c - \eta_i^c - \eta_g^c + \eta_s^c - \eta_e^{ce} - \eta_g^{ce} - \eta_e^p \quad (1)$$

where the subscripts e, i, g, and s denote the electronic, ionic, gas-phase, and activation components of the overpotentials, and the superscripts ae, a, m, c, ce, and p represent the anode electrode (gas diffusion layer), anode catalyst, membrane, cathode catalyst, cathode electrode (gas diffusion layer), and the bipolar plate, respectively.

The method of calculating the various overpotentials in Eq. (1) has been described in Refs. [2,3] and will not be repeated. Here, we discuss the development of a method to determine the effect of CO and CO_2 impurities on the anode overpotential, η_s^a.

2.1. Poisoning model

In our model, the kinetics of the hydrogen oxidation reaction (HOR) are described by considering dissociative adsorption of H_2 on Pt sites followed by electrochemical oxidation of the adsorbed H_2 species.

$$H_2 + 2M \underset{k_H^d}{\overset{k_H^a}{\rightleftarrows}} 2M - H \quad \text{(R-1)}$$

$$M - H \xrightarrow{k_H^e} M + H^+ + e^- \quad \text{(R-2)}$$

Camara et al. [4] have shown that both linearly bonded and bridge-bonded species must be considered in order to explain the experimental data on CO poisoning of Pt electrocatalyst. Our analysis suggests that the low CO concentration data can be adequately explained by considering only the bridge-bonded sites. Since our interest is in Pt poisoning at low CO concentrations, the model can be simplified by considering associative adsorption of CO on bridge sites and electrochemical oxidation of bridge-bonded CO.

$$CO + 2M \underset{k_{CO}^d}{\overset{k_{CO}^a}{\rightleftarrows}} M_2 - CO \quad \text{(R-3)}$$

$$M_2 - CO + H_2O \xrightarrow{k_{CO}^e} 2M + CO_2 + 2H^+ + 2e^- \quad \text{(R-4)}$$

Analyses by Janssen [5] and others indicate that the effect of CO_2 on cell polarization data can be simulated by considering the catalytic reverse water–gas shift reaction (RWGS). Consistent with reactions (R-3) and (R-4), we include the following reaction between the adsorbed H_2 species and gaseous CO_2 to produce bridge-bonded CO.

$$CO_2 + 2M - H \xrightarrow{k_{CO_2}^r} M_2 - CO + H_2O \quad \text{(R-5)}$$

For very low CO concentrations and thin membranes, enough O_2 may cross over from the cathode air to affect the site balance. We model the effect of this internal oxygen bleed by including the competitive oxidation of the adsorbed CO species and H_2 species.

$$M_2 - CO + \frac{1}{2}O_2 \xrightarrow{k_{CO}^s} 2M + CO_2 \quad \text{(R-6)}$$

$$2M - H + \frac{1}{2}O_2 \xrightarrow{k_H^s} 2M + H_2O \quad \text{(R-7)}$$

We define θ_M, θ_H and θ_{CO} as the fractions of Pt sites that are, respectively, vacant, occupied by H and occupied by CO. We assume that there is only one type of site and that all sites can be bridge-bonded by CO. It is further assumed that the reaction order is the same as the molecularity for all species in reactions (R-1) through (R-7), except O_2 in reactions (R-6) and (R-7) for which the reaction order is taken as 1 rather than 1/2. Analysis of experimental data showed a better match with theory if the reaction order is taken as 1.5 for M−H in reaction (R-2) and CO_2 in reaction (R-5). With these assumptions, the steady-state site coverage can be determined by solving the following set of algebraic equations:

$$2k_H^a P_{H_2}^a \theta_M^2 - 2k_H^d \theta_H^2 - 2k_H^e \theta_H^{1.5} \sinh\left(\frac{\alpha_H z_H F \eta_a}{RT}\right) - 2k_{CO_2}^r (P_{CO_2}^a)^{1.5} \theta_H^2 - 2k_H^s \theta_H^2 P_{O_2}^a = 0 \quad (2)$$

$$2k_{CO}^a P_{CO} \theta_M^2 \exp\left(\frac{-\beta r \theta_{CO}}{RT}\right) - 2k_{CO}^d \theta_{CO} \exp\left(-\frac{(1-\beta) r \theta_{CO}}{RT}\right) - 2k_{CO}^e \theta_{CO} \sinh\left(\frac{\alpha_{CO} z_{CO} F \eta_a}{RT}\right) + 2k_{CO_2}^r (P_{CO_2}^a \theta_H^2)^{1.5} - 2k_{CO}^s \theta_{CO} P_{O_2}^a = 0 \quad (3)$$

In writing Eqs. (2) and (3) we have further assumed that the kinetics of the electrochemical oxidation reactions can be described by Butler–Volmer type equations. Also, a correction factor has been applied to CO adsorption and desorption rates as per the Temkin adsorption isotherm [6].

Knowing site coverages and reaction rates, the variation of the molar flow rates of H_2, N_2, CO, CO_2, O_2 and H_2O along the flow direction can be determined from the following conservation equations:

$$\frac{d\dot{N}_{H_2}}{dA} = -\frac{J_H}{2F} - \frac{\psi_{H_2} P_{H_2}^a}{\delta_m} - N_c k_H^s \theta_H^2 P_{O_2}^a - N_c k_{CO_2}^r P_{CO_2}^a \theta_H^2 \quad (4)$$

$$\frac{d\dot{N}_{N_2}}{dA} = \frac{\psi_{N_2}(P_{N_2}^c - P_{N_2}^a)}{\delta_m} \quad (5)$$

$$\frac{d\dot{N}_{O_2}}{dA} = \frac{\psi_{O_2} P_{O_2}^c}{\delta_m} - 1/2 N_c (k_{CO}^s \theta_{CO} P_{O_2}^c + k_H^s \theta_H^2 P_{O_2}^a) \quad (6)$$

$$\frac{d\dot{N}_{CO}}{dA} = N_c \left[-k_{CO}^a P_{CO} \theta_M^2 \exp\left(\frac{-\beta r \theta_{CO}}{RT}\right) + k_{CO}^d \theta_{CO} \exp\left(-\frac{(1-\beta) r \theta_{CO}}{RT}\right)\right] \quad (7)$$

$$\frac{d\dot{N}_{CO_2}}{dA} = N_c \left(k_{CO}^e \theta_{CO} \sinh\left(\frac{\alpha_{CO} z_{CO} F \eta_a}{RT}\right) + k_{CO}^s \theta_{CO} P_{O_2}^a - k_{CO_2}^r (P_{CO_2}^a)^{1.5} \theta_H^2\right) \quad (8)$$

$$\frac{d\dot{N}_{H_2O}}{dA} = -\frac{\alpha_m J_H}{F} + N_c (k_{CO_2}^r \theta_H^2 (P_{CO_2}^a)^{1.5} + k_H^s \theta_H^2 P_{O_2}^a) \quad (9)$$

In the above equations, the current density is related to the electrochemical oxidation rates as

$$J_H = 2F N_c k_H^e \theta_H^{1.5} \sinh\left(\frac{\alpha_H z_H F \eta_a}{RT}\right) \quad (10)$$

$$J_{CO} = 2F N_c k_{CO}^e \theta_{CO} \sinh\left(\frac{\alpha_{CO} z_{CO} F \eta_a}{RT}\right) \quad (11)$$

$$J = J_H + J_{CO} \quad (12)$$

2.2. Method of solution

An implicit finite-difference scheme was used to solve the governing equations. The fuel cell was divided into 5–50 axial

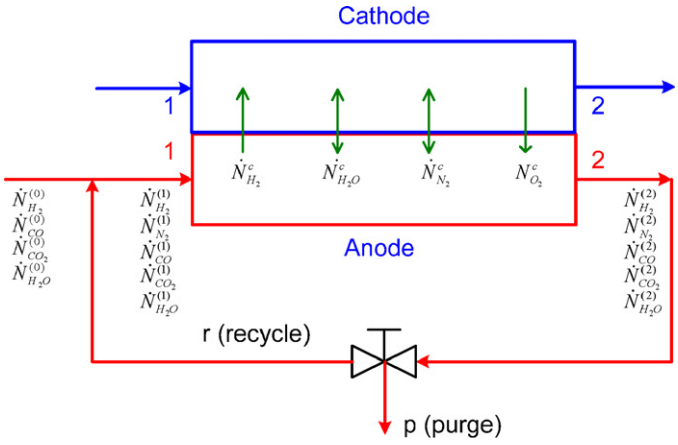

Fig. 1. Anode gas recycle with partial purge.

nodes and a marching algorithm was used to solve the resulting non-linear algebraic equations from cell inlet to outlet. The solution was iterative because of the recycle loop that couples the anode inlet boundary conditions: (1) to the gas compositions of fuel H_2 (0) and the anode effluent (2) as shown in Fig. 1.

$$\dot{N}_j^{(1)} = \dot{N}_j^{(0)} + (1 - f_p)\dot{N}_j^{(2)}, \tag{13}$$

where $j = H_2$, N_2, CO, CO_2 or O_2.

A simple fixed-point iteration method was used to carry out the iterations. Usually, fewer than 100 iterations were needed to achieve convergence to any desired accuracy.

3. Model validation

Extensive data is available in the literature that could be used to validate the CO/CO_2 poisoning model presented in Section 2. We specifically selected data to validate the models for CO poisoning as functions of CO concentration and temperature, effect of O_2 in relieving the CO poisoning and reverse water gas reaction between adsorbed CO and gaseous O_2.

Table 1 summarizes our choice of rate and model constants for the adsorption, desorption, electrochemical oxidation, RWGS and surface oxidation steps in reactions (R-1) through (R-7). The constants in Table 1 are given for 85 °C temperature (T_{ref}) and have been either taken from literature or derived from data fitting. The rate constants for the adsorption steps are scaled with respect to temperature based on the kinetic theory of gases applied to molecular collisions with surfaces and for the desorption steps on the basis of the heat of desorption.

$$k_i^a = k_{i,ref}^a \left(\frac{T_{ref}}{T}\right)^{0.5}, \tag{14}$$

$$k_i^d = k_{i,ref}^d \exp\left(\frac{\Delta H_i^d}{R}\left(\frac{1}{T_{ref}} - \frac{1}{T}\right)\right), \tag{15}$$

where i denotes H in reaction (R-1) and CO in reaction (R-3). We have inferred a ΔH_H^d of 9.5 kJ mol^{-1} and a ΔH_{CO}^d of 150 kJ mol^{-1} from the analysis of the selected data which is in agreement with the data reported in Ref. [7].

Table 1
Model constants derived from experimental data reported in Refs. [1,4,8,9]

Variable	Unit	
k_H^a	mol/(m_{Pt}^2 bar)	0.01
$k_{H,ref}^d$	mol/m_{Pt}^2	0.005
k_H^e	mol/m_{Pt}^2	0.02
k_H^s	mol/(m_{Pt}^2 bar)	9.5
k_{CO}^a	mol/(m_{Pt}^2 bar)	0.005
$k_{CO,ref}^d$	mol/m_{Pt}^2	5×10^{-15}
$k_{CO,ref}^e$	mol/m_{Pt}^2	6×10^{-10}
$k_{CO_2,ref}^r$	mol/(m_{Pt}^2 bar$^{1.5}$)	3.8×10^{-10}
$k_{CO,ref}^s$	mol/(m_{Pt}^2 bar)	2.9×10^{-4}
β		0.1
α_H		0.5
α_{CO}		0.15
T_{ref}	K	358
ΔH_H^d	kJ mol^{-1}	9.5
ΔH_{CO}^d	kJ mol^{-1}	150
E_{CO}^e	kJ mol^{-1}	65
$E_{CO_2}^r$	kJ mol^{-1}	85
E_{CO}^i	kJ mol^{-1}	39.7
z_H		1
z_{CO}		2

The rate constants for the electrochemical oxidation steps are scaled with respect to temperature based on the activation energy.

$$k_i^e = k_{i,ref}^e \exp\left(\frac{E_i^e}{R}\left(\frac{1}{T_{ref}} - \frac{1}{T}\right)\right) \tag{16}$$

We have inferred a value of 65 kJ mol^{-1} for E_{CO}^e from the literature data on effect of temperature on degradation of cell potential due to CO. We currently do not have a recommendation for E_H^e.

The rate constant for the RWGS reaction has been scaled with respect to temperature using 85 kJ mol^{-1} activation energy ($E_{CO_2}^r$). At present, we do not have a recommendation for the temperature dependence of k_H^s or k_{CO}^s. More data on temperature dependence of recovery from CO poisoning by air bleed is needed to refine the choice of rate constants for the oxidation reactions (R-6) and (R-7).

Finally, catalyst site density (mol-Pt/m^2) is related to the Pt loading (L_{Pt}) and the specific electrochemical surface area of Pt (A_{Pt}^0) as

$$N_c = 2.2 \times 10^{-5} L_{Pt} A_{Pt}^0, \tag{17}$$

which is based on 210 μC cm^{-2}-Pt as the charge that Pt can hold. Gasteiger et al. [10] recommend a value of 52 m^2 g^{-1} for A_{Pt}^0 for optimized electrode structures.

Figs. 2 and 3 compare the modeled dependence of anode overpotential on CO concentration and temperature with the single-cell experimental data of Lee et al. [1] The MEA consisted of Nafion 115 membrane with 0.4 mg cm^{-2} Pt loading on anode and cathode (0.8 mg cm^{-2} total Pt loading). The cell was operated with H_2/O_2 and H_2–CO/O_2, maintaining 1-bar partial pressure of H_2 and O_2 in humidified anode and cathode streams. Within the range of CO concentrations analyzed, Fig. 2

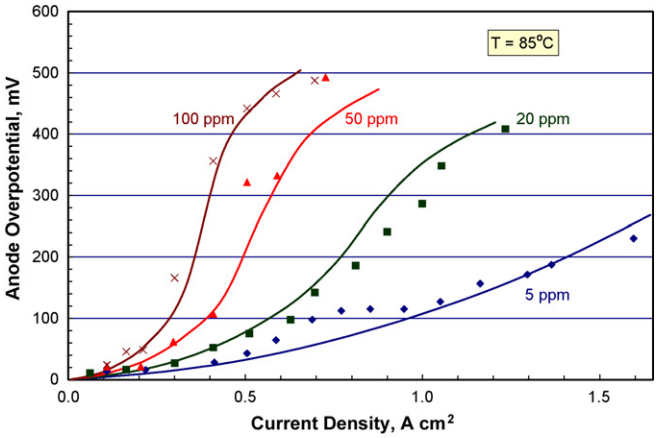

Fig. 2. Model validation: effect of CO on anode overpotential at 85 °C. Symbols denote experimental data from Ref. [1].

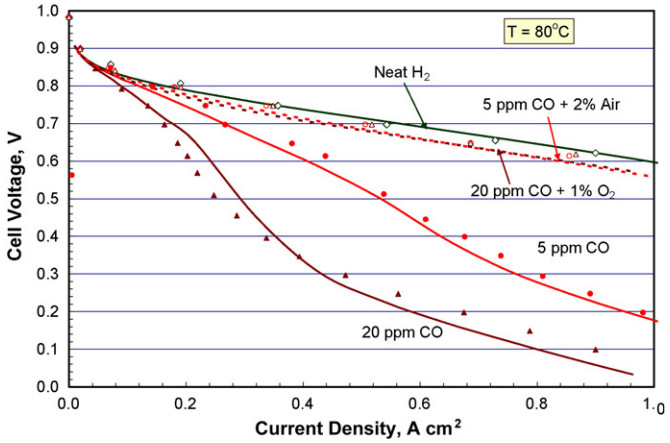

Fig. 4. Model validation: effect of air bleed on anode overpotential at 80 °C. Symbols denote experimental data from Ref. [8] (empty diamonds, neat H_2; empty squares, 5 ppm CO with 2% air; empty triangles, 20 ppm CO with 1% O_2; filled squares, 5 ppm CO; filled triangles, 20 ppm CO).

shows good agreement between the anode overpotential calculated using the bridge-site assumption and the experimental data at 85 °C. Fig. 3 shows that for 20-ppm CO in fuel H_2, the assumption of 150 kJ mol^{-1} for ΔH^{d}_{CO} gives good agreement between the calculated and measured anode overpotentials over the temperature range 70–100 °C although some disparity is observed at 40 °C.

Experimental data of Wilson et al. [8] was selected to validate the choice of rate constants for CO and H_2 oxidation reactions over Pt. These experiments were conducted with Nafion 105 membrane and a low 0.14 mg cm^{-2} Pt loading on anode and cathode. The cell was operated with humidified anode and cathode streams at 80 °C and 1 bar. Fig. 4 presents the modeled polarization curves for neat H_2, 5-ppm CO in H_2 and 20-ppm CO in H_2, and compares them with the experimental data. It also includes modeled curves with 2% air bleed in H_2 containing 5 ppm CO and curves with 1% O_2 bleed in H_2 containing 20 ppm CO. In both cases, the choice of rate constants, k^{s}_{H} and k^{s}_{CO}, listed in Table 1, is seen to yield an excellent match with the measured voltage recovery with air/oxygen bleed.

Experimental data of Gu et al. [9] were selected to validate the CO_2 degradation model. These experiments were conducted using the Primea MEA, Series 5510 that has a 25-μm thick gore-select membrane and catalyst loadings of 0.4 mg cm^{-2} Pt on both anode and cathode. The cell was operated at 70 °C and 1 bar, with the anode and cathode gases humidified to 80 and 70 °C dew point temperatures, respectively. The stoichiometry was 1.2 for the anode (83% H_2 utilization) and 2.0 for cathode (50% O_2 utilization). Fig. 5 compares the modeled and measured anode overpotential, defined as the difference between the cell voltage with neat H_2 and the cell voltage with H_2–CO_2 mixture at the same current density. Defined in this manner, the anode overpotential includes the effect of CO_2 dilution on the Nernst potential, activation overpotential due to catalyst poisoning by CO produced by the RWGS reaction and any additional mass transfer-related overpotentials due to the presence of 20–60% CO_2. The good comparison indicates that our choice of the rate constant for the RWGS reaction ($k^{r}_{CO_2}$) in conjunction with the rate constants for CO adsorption and electrochemical oxidation reactions can explain the observed cell voltage degradation.

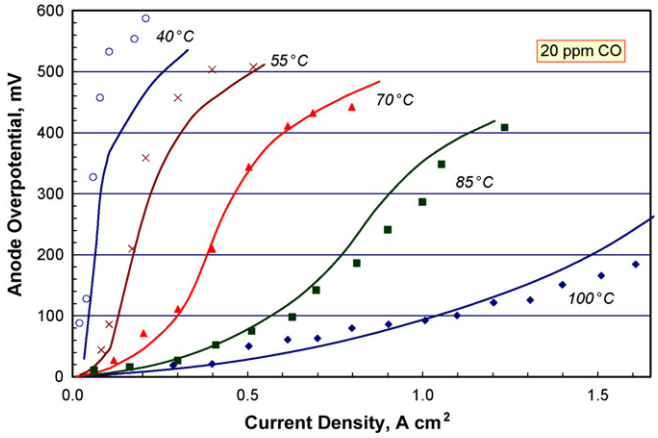

Fig. 3. Model validation: effect of temperature on anode overpotential, 20-ppm CO in fuel H_2. Symbols denote experimental data from Ref. [1].

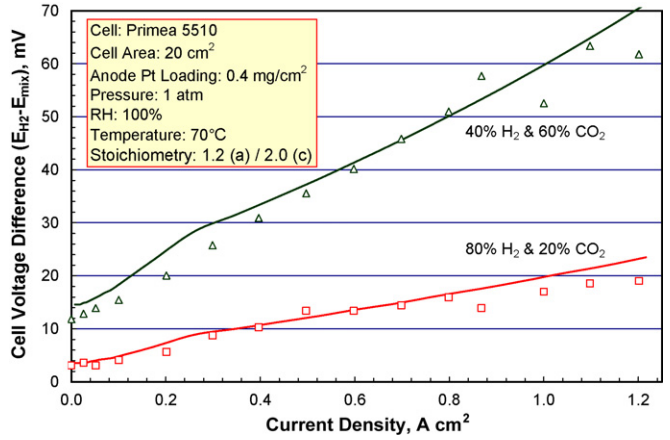

Fig. 5. Model validation: effect of 20–60% CO_2 on anode overpotential at 70 °C. Symbols denote experimental data from Ref. [9].

4. Results

Several simulations were run using the model described in Section 2 to parametrically study the effects of impurities on a reference PEFC stack that generates 90 kW_e gross (80 kW_e net system power output) in a pressurized fuel-cell system with neat H_2 as fuel [2]. Some important design and operating parameters and assumptions for the stacks are listed below.

(a) The cell voltage is 0.65 V at 90 kW_e rated power.
(b) The cell is isothermal; the cell temperature is 80 °C at all operating points.
(c) The pressure of fuel and air streams at stack inlet floats with flow rate: 2.5 bar at rated flow, 2.0 bar at 75% flow, 1.5 bar at 50% flow, 1.3 bar at 25% flow and 1.1 bar at 10% flow. The air management system has a maximum turndown of 20.
(d) The stack operates at 50% O_2 utilization and 70% per-pass H_2 utilization if the air management system can match the airflow rate required for a given electrical load. For stack operation below the maximum turndown of the air management system, the O_2 utilization is less than 50% and the H_2 flow rate in the anode channels is held constant. In this operating regime, both the O_2 and the H_2 utilization decrease as the electrical load is reduced.
(e) Both anode and cathode inlet gas streams are humidified to 60% relative humidity (RH) at 80 °C stack temperature, i.e., the dew point temperature is 68 °C.
(f) The membrane electrode assembly (MEA) consists of a 25-μm thick PFSA membrane whose physical and transport properties (density, water uptake, swelling, ionic conductivity, osmotic drag and water diffusivity) are given by correlations available for Nafion 112. The anode and cathode catalyst layers have identical electrode structures: 0.4 mg cm^{-2} Pt loading, Pt/C = 0.47, ionomer/C = 0.8, 54 m^2 g^{-1}-Pt electrochemical surface area, and 40% porosity. It is assumed that the kinetics of the electrochemical oxygen reduction reaction over Pt can be adequately described using the parameters (exchange current density, transfer coefficients, etc.) derived by Gasteiger et al. [10].

Fig. 6 shows the modeled polarization curve for a single cell of the stack with neat H_2 as fuel. It includes performance losses due to crossover of H_2, O_2, and N_2 across the membrane. The recycle ratio is 125 (0.8% purge) to control the buildup of N_2 in the anode gas channels.

4.1. Effect of recycle

Fig. 6 also presents the combined effects of CO impurity and anode gas recycle on the polarization curves. Two sets of calculated results are included in Fig. 6 ($R = 0$ and 100) to isolate the effect of CO in fuel H_2 from the effect of CO buildup in the recycled anode gas. The polarization curve for $R = 0$ (once-through anode gas flow) indicates that 1-ppm CO in fuel H_2 decreases the cell voltage by 35 mV at 1.05 A cm^{-2}. The polarization curve

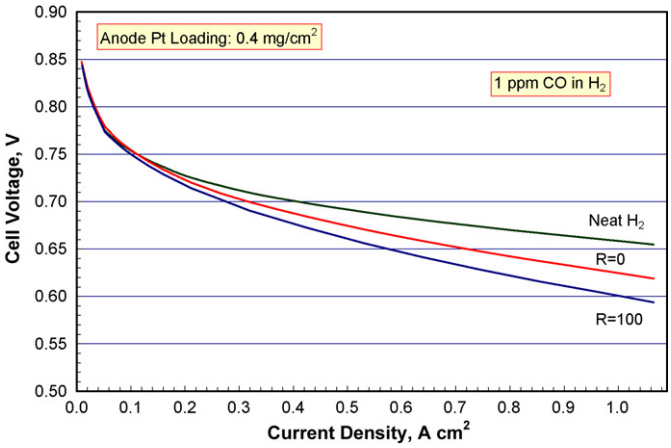

Fig. 6. Effect of anode gas recycle on voltage degradation due to CO in fuel H_2.

for $R = 100$ (closed anode circuit, 1% purge) shows a further decrease of 25 mV at 1.05 A cm^{-2} because of CO buildup due to anode gas recycle.

Our simulations suggest that above a certain threshold that is determined by O_2 crossover, even a small concentration of CO in fuel H_2 can cause a measurable decrease in cell voltage at a high enough recycle.

Analogous to Fig. 6 for CO, Fig. 7 presents the effects of CO_2 impurity and anode gas recycle on the polarization curves. The polarization curve for $R = 10$ shows that 1% CO_2 in fuel H_2 decreases the cell voltage by 15 mV at 1.05 A cm^{-2}. The cell voltage decreases by 50 mV if the recycle is increased to 100. Our simulations suggest that at small recycle ratios, the decrease in cell voltage is primarily due to production of CO by the reverse water–gas shift reaction. At large recycle ratios, the decrease in Nernst potential due to the lowering of the H_2 partial pressure by buildup of CO_2 also comes into play.

4.2. Degradation mechanism

Fig. 8 has been constructed to clarify the modeled mechanism of performance degradation due to CO and CO_2 impurities. Fig. 8a displays the isotherm for H_2 adsorption on the Pt elec-

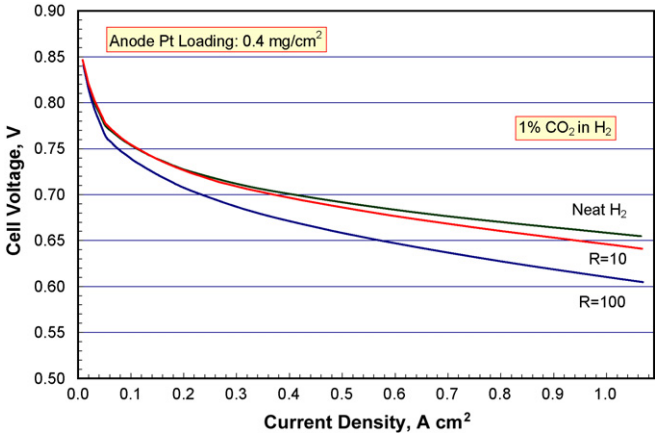

Fig. 7. Effect of anode gas recycle on voltage degradation due to CO_2 in fuel H_2.

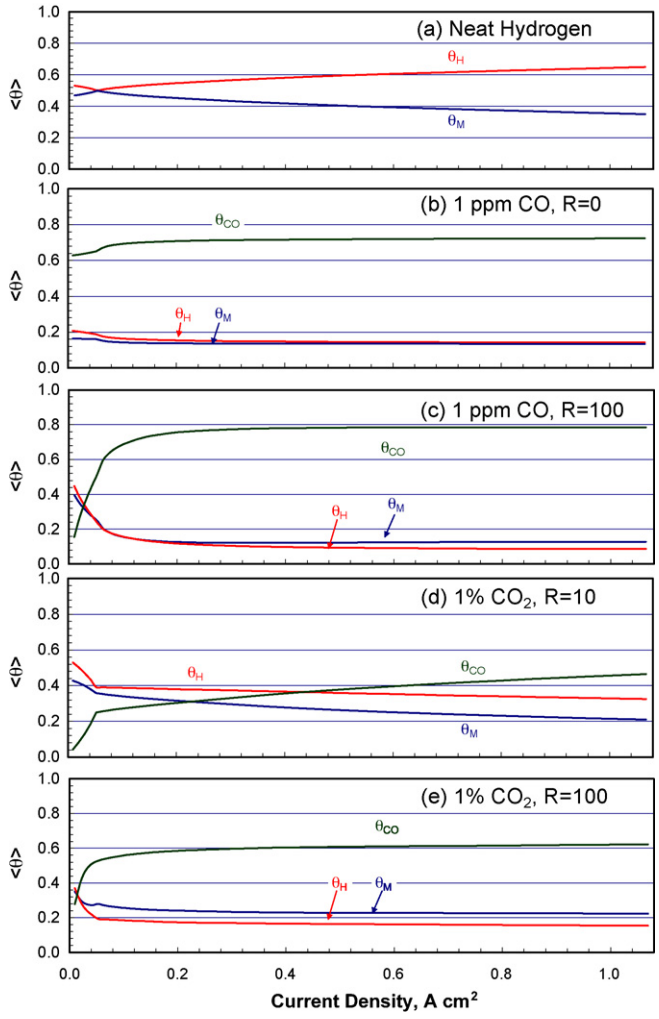

Fig. 8. Average site coverage under different operating conditions.

trocatalyst. At low current densities, the calculated average H_2 coverage ($\langle\theta_i\rangle = \int\theta_i\, dA/A$) is greater than 45%. In Fig. 8a, $\langle\theta_H\rangle$ increases with current density because of the coincident increase in the operating pressure that causes the adsorption equilibrium in reaction (R-1) to shift to the right. At constant pressure, $\langle\theta_H\rangle$ should decrease with increase in current density because of the faster rate of the H_2 oxidation reaction.

Fig. 8b ($R=0$) indicates that CO adsorbs strongly on Pt ($<\theta_{CO} \gg 0.7$ at 0.5 A cm^{-2} and higher current densities) and blocks the access of H_2 to the catalytic sites. It shows that 1-ppm CO at 80 °C can reduce $\langle\theta_H\rangle$ to <0.2 from >0.6 with neat H_2. Fig. 8c indicates that $\langle\theta_{CO}\rangle$ may approach 0.8 with anode gas recycle ($R=100$), causing $\langle\theta_H\rangle$ to decrease to <0.1.

Our model indicates that whereas HOR is confined near the membrane–catalyst interface with neat H_2, it spreads out towards the catalyst–gas diffusion medium interface in the presence of CO. Our simulations show that the HOR becomes more uniform and the catalyst utilization improves as $\langle\theta_{CO}\rangle$ increases.

Fig. 8d and e present the adsorption isotherms in the presence of CO_2 in fuel H_2. CO_2 adsorbs weakly on Pt but can produce CO by the catalytic reverse water–gas shift reaction. For this reason, the adsorption isotherms with CO_2 impurity are qualitatively similar to those with CO impurity except that much larger concentrations of CO_2 and high recycle ratios are needed to produce similar changes in $\langle\theta_{CO}\rangle$ and $\langle\theta_H\rangle$.

4.3. Optimum recycle

A parametric study was conducted to characterize the degradation in stack performance due to CO impurity in fuel H_2. It was found that the stack efficiency (η) is a useful metric for characterizing the performance degradation. Here η is defined as the ratio of the dc power generated by the stack to the lower heating value (LHV) of H_2 utilized in the electrochemical reaction, H_2 that reacts in the cathode due to crossover from the anode, H_2 that reacts in the anode with O_2 that crosses over from the cathode, and H_2 that is purged from the anode recycle loop. The results of the study are summarized in Fig. 9, which shows that for a given set of operating conditions, there exists an optimum recycle (R^*) at which the stack efficiency (η^*) is maximum. The stack efficiency is lower than η^* for $R<R^*$ because of the excessive loss of H_2 in purge gas. The stack efficiency is also lower than η^* for $R<R^*$ because of the excessive buildup of CO in the anode channels and the associated decrease in cell voltage. For the reference conditions of Section 3, R^* is 135 (0.6% purge) for neat H_2, in which case the optimum purge is determined by the crossover of N_2 to the anode from the cathode. For impure fuel H_2, R^* is a function of the CO concentration: the higher the CO concentration in fuel H_2 the lower the R^*. The optimum recycle ratio decreases from 135 for neat H_2 to 100 (1% purge) if the fuel H_2 contains 1 ppm CO.

Analogous to Fig. 9 for CO, Fig. 10 presents the optimum recycle ratios as a function of CO_2 impurity in fuel H_2. Unlike the results in Fig. 9 which show a gradual drop-off in η for $R>R^*$ and <1-ppm CO in fuel H_2, Fig. 10 shows a sharp decline in η for $R>R^*$ and >0.1% CO_2 in fuel H_2. As explained later, this is because large anode gas recycles at high enough CO_2 content can also lead to significant CO_2 buildup in the anode channel and cause the H_2 partial pressure and, therefore, the Nernst potential to decrease.

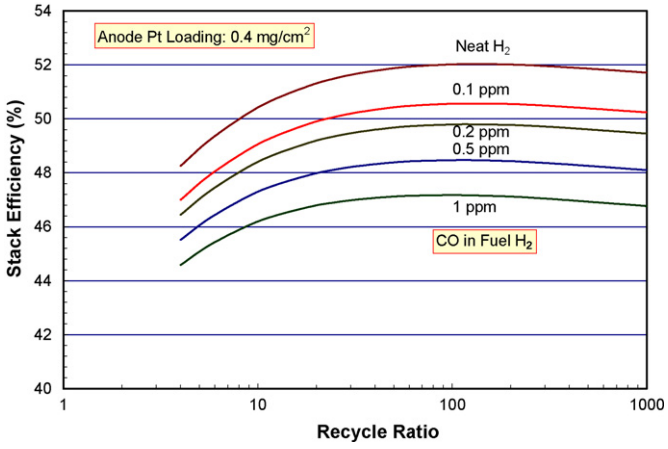

Fig. 9. Optimum recycle ratio as a function of CO concentration at 1.05 A cm^{-2}.

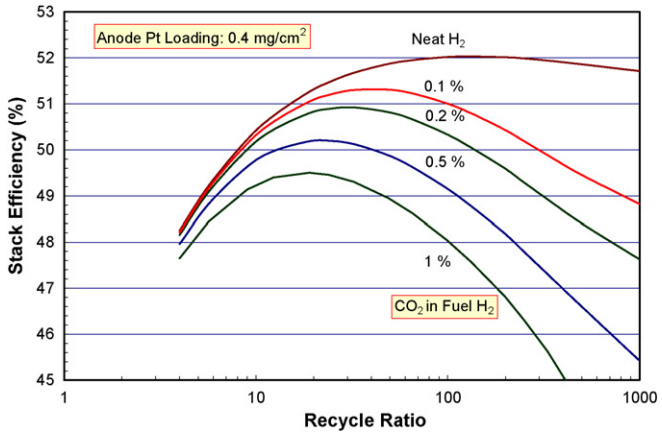

Fig. 10. Optimum recycle ratio as a function of CO_2 concentration at 1.05 A cm^{-2}.

4.4. Effect of Pt loading

Much effort is being devoted to discover new alloys and electrode structures that allow lower Pt loading and reduction in stack cost. Although the effort is primarily focused on the oxygen reduction reaction (ORR), reduction of Pt loading for the hydrogen oxidation reaction (HOR) is also of interest. To this end, a parametric study was conducted to investigate the degree to which reduction in Pt loading may adversely affect the tolerance of HOR catalyst to impurities in fuel H_2. Fig. 11 presents some representative results from a parametric study on the effect of CO impurity on efficiency of a stack with 0.05 mg cm^{-2} Pt loading. These may be compared with the results shown in Fig. 9 for 0.4 mg cm^{-2} Pt in anode catalyst to ascertain the effect of Pt loading on performance degradation due to CO impurity. The performance degradation due to reduced Pt loading is seen to be small if the fuel H_2 is free of impurities—a well known result that the H_2 oxidation reaction on Pt is facile and can be conducted at overpotentials of <5 mV, even at a Pt loading of 0.05 mg cm^{-2}.

Our simulation results suggest that under the reference operating conditions, the adverse effect of CO in fuel H_2 is amplified at low Pt loadings. At optimum recycle ratios, reducing the Pt content of the anode catalyst from 0.4 to 0.05 mg cm^{-2} causes an additional voltage drop of 24–64 mV if the fuel H_2 contains 0.1–1 ppm CO (see Table 2); the corresponding additional degradation in stack efficiency is 1.9–5.1%. Also, the lower the Pt content, the lower is the optimum recycle ratio, i.e., greater is the purge loss of H_2.

Table 2
Effect of Pt loading on degradation of cell potential and stack efficiency

Pt loading	0.4 mg cm^{-2}		0.05 mg cm^{-2}	
	ΔV	$\Delta\eta$	ΔV	$\Delta\eta$
CO (ppm)				
0.1	18.4	1.5	42.3	3.4
0.2	28.1	2.2	63.3	5.1
0.5	44.1	3.6	95.9	7.8
1.0	60.5	4.9	124.3	10.0
CO_2 (%)				
0.1	5.7	0.7	4.2	0.4
0.2	7.8	1.1	5.6	0.8
0.5	14.3	1.8	11.1	1.4
1.0	20.5	2.5	17.4	2.1

Comparison of the results in Figs. 10 and 12 suggests that reduction of Pt loading in the anode catalyst may have only a small effect on the degradation in stack efficiency due to CO_2 alone in fuel H_2. A counterintuitive result from our simulations is that, under the reference conditions, reducing the Pt content actually slows the RWGS reaction that produces the CO poison so that the cell voltage improves by 1.5–3.1 mV (see Table 2) and the stack efficiency by 0.3–0.4%.

4.5. Buildup of impurities

Fig. 13 presents the buildup of CO and CO_2 in the anode gas channels due to CO impurity in fuel H_2 when the spent anode gas is recycled to the anode inlet using the optimum recycle ratio. Fig. 13a shows the CO concentration at the stack inlet and at the stack outlet as a function of CO concentration in fuel H_2 (all concentrations reported on dry basis). A number of factors combine to determine the CO concentration profile along the

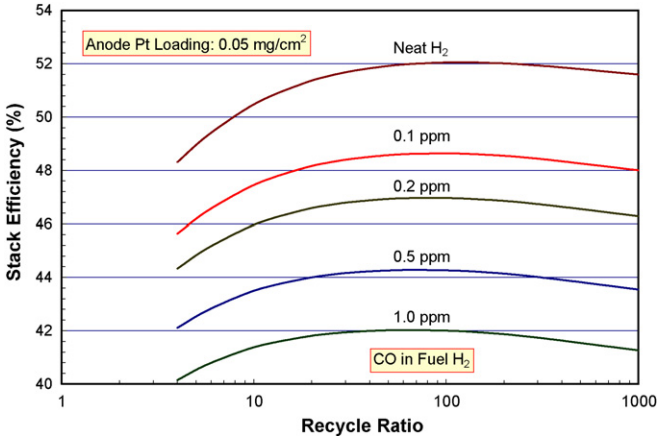

Fig. 11. Effect of CO on stack efficiency at reduced Pt loading in the anode catalyst.

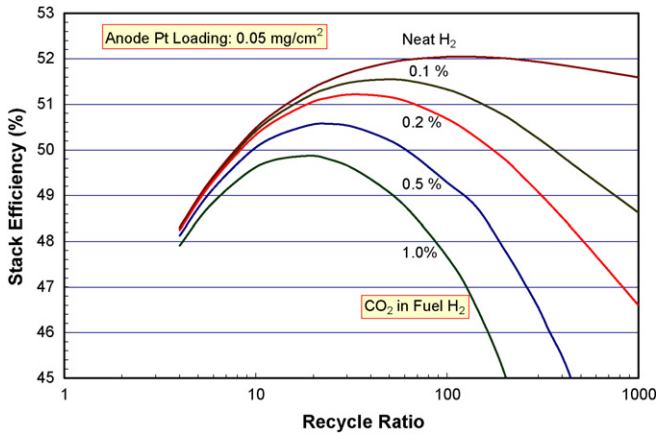

Fig. 12. Effect of CO_2 on stack efficiency at reduced Pt loading in the anode catalyst.

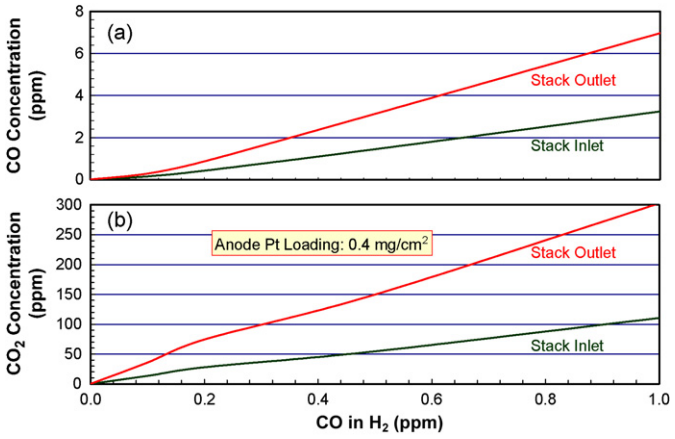

Fig. 13. CO and CO_2 buildup in anode channels due to CO in fuel H_2 at optimum recycle ratios shown in Fig. 11.

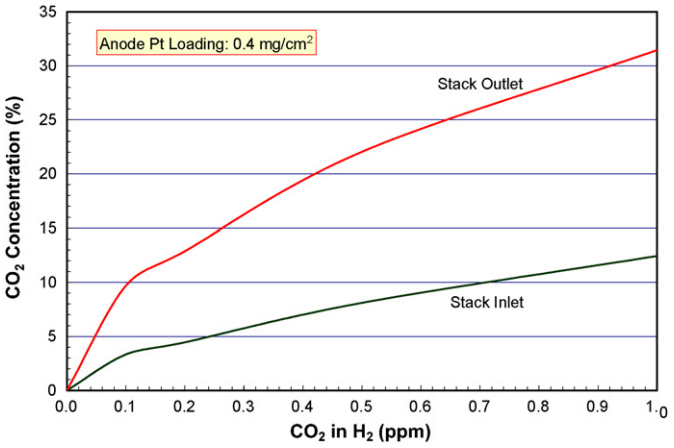

Fig. 14. Enrichment of anode gas with CO_2 at optimum recycle ratios shown in Fig. 12 (fuel H_2 contains only CO_2 impurity).

anode channel: H_2 consumption by the electrochemical reaction, electrochemical oxidation of CO, CO reaction with O_2 that crosses over from the cathode channel, CO production by RWGS reaction, etc. The results in Fig. 13a indicate that recirculation enriches the anode gas for reference stack operating conditions and optimum purge level. This implies that CO conversion to CO_2 is less than 70% (H_2 utilization) even if fuel H_2 contains 0.1 ppm CO and the amount of O_2 that crosses over is stoichiometrically sufficient to oxidize it to CO_2. This is because of low O_2 selectivity for CO oxidation if the CO coverage is small as is the case with 0.1-ppm CO concentration. O_2 selectivity for CO oxidation is higher at higher CO concentrations but the amount of O_2 crossover is stoichiometrically insufficient to oxidize it to CO_2. In our model, the primary mechanism of CO oxidation to CO_2 with 1-ppm CO in fuel H_2 is through the electrochemical step (reaction (R-4)). Fig. 13a shows that the extent of enrichment increases with CO concentration in fuel H_2. Over the 0.1–1 ppm range of CO concentration in fuel H_2, there is 45–175% enrichment in CO at stack inlet and 225–600% at stack outlet.

Fig. 13b shows that recycle can enrich the anode gas in CO_2 to a level that is more than two orders-of-magnitude higher than the concentration of CO from which it is produced by oxidation. We calculate that the fraction of CO that is converted to CO_2 is <50% if the fuel H_2 contains 0.1-ppm CO and ~20% if it contains 1-ppm CO. At these levels of CO conversion, CO will not buildup in the recycled anode gas if the stack is operated at less than 20–50% H_2 utilization.

Analogous to the results in Fig. 13 for CO, Fig. 14 presents the buildup of CO_2 in the anode gas channels due to CO_2 impurity in fuel H_2. As in Fig. 13, these results are for reference stack conditions and optimum recycle ratios but with no CO in fuel H_2. Note that anode gas recycle can enrich the gas in CO_2 by a factor of 10 at stack inlet and 30 at stack outlet (Fig. 14).

4.6. Impurity limits

A parametric study was conducted to determine the decrease in cell voltage and degradation in stack efficiency as a function

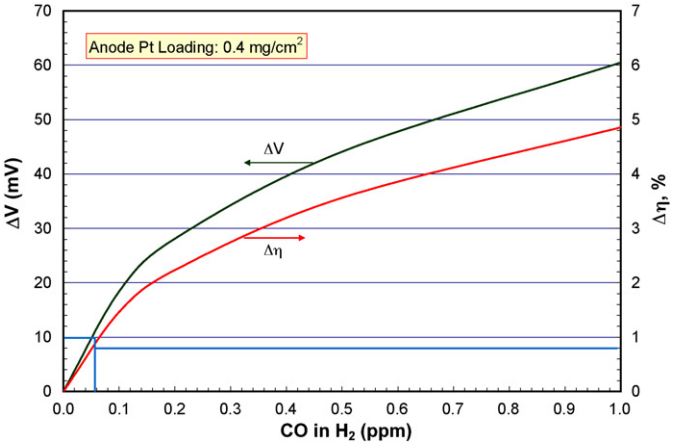

Fig. 15. Relationship between CO impurity in fuel H_2 and degradation in cell voltage and stack efficiency at reference conditions.

of impurity concentration in fuel H_2. Figs. 15 and 16 present the results of the study for reference stack conditions, current density (1.05 A cm^{-2}) that leads to 0.65-V cell voltage with neat H_2 after accounting for N_2 crossover, and optimum

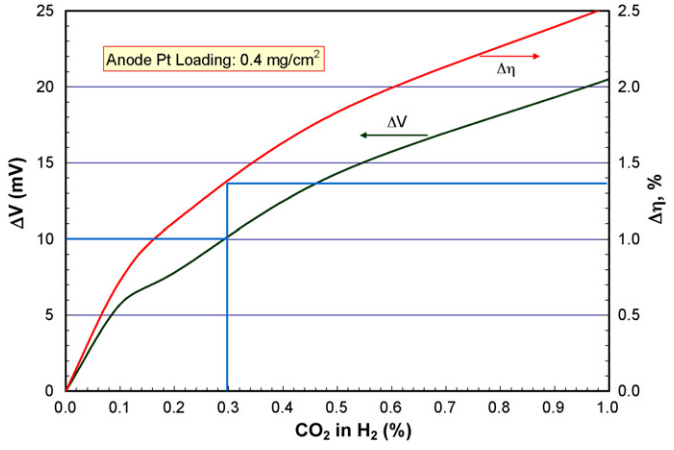

Fig. 16. Relationship between CO_2 impurity in fuel H_2 and degradation in cell voltage and stack efficiency at reference conditions.

recycle ratios. These results, which may be useful in developing H_2 quality standards, can be interpreted as follows. Say that it is desired to establish the limit for CO impurity in fuel H_2 on the basis that the maximum decrease in cell voltage at 1.05 A cm^{-2} should be restricted to 10 mV. Fig. 15 suggests that the CO concentration then has to be limited to <0.06 ppm and that the corresponding degradation in cell efficiency would be ∼0.8%-point. The optimum recycle ratio at this operating condition would be about 100, see Figs. 9 and 13 indicates that with 0.06 ppm CO in fuel H_2, anode gas recycle does not cause significant enrichment in CO because of its oxidation by O_2 crossover through the 25-μm membrane. As a point of reference, Fig. 15 suggests that 1-ppm CO in fuel H_2 would cause >60 mV decrease in cell voltage and ∼5 percentage-point degradation in stack efficiency. Fig. 13 indicates that anode gas recycle with 1-ppm CO in fuel H_2 (optimum $R < 100$ in Fig. 9) builds up CO level to >3 ppm at stack inlet and ∼7 ppm at stack outlet.

Applying the above criterion to CO_2, Fig. 16 suggests that the CO_2 concentration in fuel H_2 needs to be <3000 ppm in order to limit the decrease in cell voltage to 10 mV at 1.05 A cm^{-2}. The corresponding degradation in stack efficiency is ∼1.4%-point and the optimum recycle ratio from Fig. 10 is about 30. Fig. 14 indicates that a recycle ratio of 30 would enrich the anode gas from 2500 ppm CO_2 in fuel H_2 to a CO_2 concentration of 5% at stack inlet and 14% at stack outlet.

Note that the results in Figs. 15 and 16 are applicable to one set of design and operating conditions. The decrease in cell voltage and degradation in stack efficiency due to CO and CO_2 impurities depends on many parameters such as the operating pressure and temperature, membrane thickness and Pt loading in the anode electrocatalyst. The effects of these parameters will be explored in a future publication.

5. Conclusions

We have conducted a comprehensive study on the effect of CO and CO_2 impurities in fuel H_2 on the performance of a pressurized PEFC stack for automotive applications. The major conclusions from the analysis in response to the questions posed in Section 1 are briefly summarized below:

- Any CO impurity in the fuel adsorbs strongly on the Pt catalyst and degrades the cell voltage by blocking the access of H_2 to the catalyst sites. At low CO concentrations, <100 ppm, the observed degradation can be explained on the basis of bridge-site adsorption of CO, followed by electrochemical oxidation of CO to CO_2.
- Any CO_2 impurity in the fuel adsorbs weakly on the Pt catalyst. At low CO_2 concentrations, the observed degradation in cell voltage can be explained on the basis of CO produced by the reverse water–gas shift reaction between CO_2 and the adsorbed H_2. At higher CO_2 concentrations, the decrease in cell potential due to dilution of the H_2 also contributes to performance degradation.
- At high H_2 utilization, depending on O_2 crossover and current density, anode gas recycle can enrich the recirculating gas with CO impurity. Recycle always leads to buildup of CO_2 in the anode channels.
- The buildup of CO and CO_2 impurities can be controlled by purging a fraction of the spent anode gas. There is an optimum purge level at which the degradation in the stack efficiency is the smallest. The stack efficiency is lower for purge higher than the optimum because of excessive loss of H_2 in purge gas. The stack efficiency is also lower for purge less than the optimum because of the decrease in cell voltage due to the excess buildup of CO and CO_2.
- The method and results presented in this paper can be used to determine the limits of CO and CO_2 impurities in fuel H_2. The impurity limits are functions of stack design and operating conditions and allowable degradation in cell voltage and stack efficiency. As an example, Fig. 15 indicates that CO concentration in fuel H_2 should be less than 0.06 ppm if the decrease in cell voltage of the reference stack is to be restricted to 10 mV at rated power. At this concentration, the optimum recycle ratio is about 100 and the stack efficiency degrades by ∼0.8 percentage-point. Under the same restriction, the CO_2 concentration should be less than 2500 ppm for a corresponding decrease of ∼1.3 percentage-point decrease in stack efficiency at an optimum recycle ratio of ∼40.

Acknowledgements

This work was supported by the U.S. Department of Energy's Office of Energy Efficiency and Renewable Energy. Dr. Nancy Garland and Mr. Jason Marcinkoski of the Office of Hydrogen, Fuel Cells, and Infrastructure Technologies are the Technology Development Managers for this study. The authors thank Dr. Romesh Kumar of Argonne National Laboratory for many useful discussions and helpful suggestions.

Argonne National Laboratory, a U.S. Department of Energy Office of Science laboratory, is operated by UChicago Argonne, LLC, under contract no. DE-AC02-06CH11357.

References

[1] S.J. Lee, S. Mukerjee, E.A. Ticianelli, J. McBreen, J. Electrochem. Acta 44 (1999) 3283–3293.
[2] R.K. Ahluwalia, X. Wang, J. Power Sources 162 (2006) 502–512.
[3] R.K. Ahluwalia, X. Wang, J. Power Sources 171 (2007) 63–71.
[4] G.A. Camara, E.A. Ticianelli, S. Mukerjee, S.J. Lee, J. McBreen, J. Electrochem. Soc. 149 (2002) A748–A753.
[5] G.J.M. Janssen, J. Power Sources 136 (2004) 45–54.
[6] T.E. Springer, T. Rockward, T.A. Zawodinski, S. Gottesfeld, J. Electrochem. Soc. 148 (2001) A11–A23.
[7] J.C. Davis, et al., Fuel Cells 4 (2004) 309–319.
[8] M.S. Wilson, C.R. Derouin, J.A. Valerio, S. Gottesfeld, Proc. 28th Intersociety Energy Conversion Engineering Conf, Vol. 1, Georgia, Atlanta, 1993, pp. 1203–1208.
[9] T. Gu, W.-K. Lee, J.W. Van Zee, M. Murthy, J. Electrochem. Soc. 151 (2004) A2100–A2105.
[10] H.A. Gasteiger, J.E. Panels, S.G. Yan, J. Power Sources 127 (2004) 162–171.